Contribution from the Institut für Physikalische und Theoretische Chemie
and Institut für Anorganische Chemie, Universität Regensburg, D-8400 Regensburg, Federal Republic of Germany

Luminescence at High Pressures and Magnetic Fields and the Structure of Single-Crystal Platinum(II) Binuclear Complexes $M_x[Pt_2(POP)_4]\cdot nH_2O$ ($M_x = Ba_2$, $[NH_4]_4$; POP = $P_2O_5H_2^{2-}$)

Ludwig Bär,[†] Helmut Englmeier,[†] Günter Gliemann,*[,†] Ulrich Klement,[‡] and Klaus-Jürgen Range*[,‡]

Received July 5, 1989

The polarized emission spectra of single-crystal $[NH_4]_4[Pt_2(P_2O_5H_2)_4]$ as functions of temperature (1.9 K $\leq T \leq$ 295 K), high static pressure (1 bar $\leq p \lesssim$ 60 kbar), and homogeneous magnetic fields ($0 \leq H \leq 6$ T) are reported and compared with corresponding spectra of single-crystal $Ba_2[Pt_2(P_2O_5H_2)_4]\cdot 8H_2O$. The differences of the emission properties can be traced back to differences of the crystal structures of the compounds. Crystallographic data for $Ba_2[Pt_2(P_2O_5H_2)_4]\cdot 8H_2O$: monoclinic, space group *Pc*, $a = 9.5452$ (8) Å, $b = 19.459$ (2) Å, $c = 7.6611$ (8) Å, $\beta = 90.758$ (8)°, $V = 1422.8$ Å^3, $Z = 2$, $d_c = 3.23$ g·cm^{-3}, $d_o > 2.9$ g·cm^{-3}, μ(Mo Kα) = 131.7 cm^{-1}, $R = 0.021$ and $R_w = 0.027$ for 321 variables and 3284 unique reflections with $I > 3\sigma(I)$. For the ammonium compound the optical properties indicate a structural arrangement of the complex anions, as observed for the potassium compound (space group $P\bar{4}b2$). With increasing pressure the single-crystal phosphorescence of both compounds is red shifted. $[NH_4]_4[Pt_2(P_2O_5H_2)_4]$ shows an additional, pressure-induced emission band at lower energy. It can be assigned to emission centers, which are formed by the approach of two binuclear units.

Introduction

The photophysical and photochemical properties of binuclear d^8–d^8 systems have focused much recent research. Examples are the rhodium(I) complexes $[Rh_2(bridge)_4]^{2+}$ (bridge = μ-η^2-1,3-diisocyanopropane)[1-6] and $[Rh_2(TBM)_4]^{2-}$ (TBM = μ-η^2-2,5-dimethyl-2,5-diisocyanohexane),[7] and the iridium(I) system $Ir_2(pz)_2(COD)_2$ (pz = μ-η^2-pyrazolate, COD = η^4-1,4-cyclooctadiene).[8,9] Much attention has been attracted by such platinum(II) compounds, which have the tendency to form dimeric or larger oligomeric units. Several of these compounds as the tetracyanoplatinates(II)[10] and *cis*-bis(2-phenylpyridine)platinum(II) (≡CBPPP)[11-13] exist as monomers in diluted solutions. In aqueous solutions at high concentrations and at high pressures and in the crystalline state the $[Pt(CN)_4]^{2-}$ ions form oligomeric units[14,15] and columns,[10] respectively. For CBPPP binuclear units have been proved only for the solid state.[11] In another class of platinum(II) compounds there are binuclear units both in the dissolved state and in the crystalline state. Examples of this class are the extensively studied d^8–d^8 systems $M_n[Pt_2(P_2O_5H_2)_4]$ (≡ M–POP), with $M_n = K_4$, Ba_2, $[Bu_4N]_4$, etc.[16-30] In their lowest excited triplet state these intensely luminescent compounds have an unusually short Pt–Pt distance[22-24] and act as strong reductants and oxidants.[22,30]

The optical properties of the solid M–POP's indicate different crystal structures depending on the counterion M. To find out this correlation, in the present paper the polarized emission spectra of single-crystal NH_4–POP at different temperatures and applied homogeneous magnetic fields are reported. The experimental results can be explained, if the NH_4–POP crystal is isostructural with single-crystal K–POP. For the latter it is well-known that the binuclear units form columns with a linear arrangement of the Pt–Pt axes, yielding Pt chains of alternating Pt–Pt distances of 2.925 and 5.063 Å.[31] The phosphorescence of Ba–POP, especially the polarization properties of the emission spectra,[26] however, exhibits some features different from that of NH_4–POP, pointing to differences of the arrangement of the binuclear units in both solids. For this reason the structure of single-crystal Ba–POP has been analyzed, yielding a basis for the interpretation of the spectroscopic differences.

Recently, Fetterolf et al.[32] reported on the influence of pressure on dissolved M–POP. Up to $p = 3$ kbar they observed no effect on the emission properties. As shown by Stroud et al.,[33] the triplet $d\sigma^*$–$p\sigma$ absorption of M–POP powder ground in mineral oil exhibits a pressure-induced weak blue shift. No information on the pressure dependence of the emission of single-crystal M–POP was available as yet. Thus, in a further section of our paper the emission spectra of single-crystal NH_4–POP and Ba–POP as functions of pressure at room temperature and at $T \sim 10$ K are

[†] Institut für Physikalische und Theoretische Chemie.
[‡] Institut für Anorganische Chemie.

(1) Mann, K. R.; Lewsi, N. S.; Miskowski, V. M.; Erwin, D. K.; Hammond, G. S.; Gray, H. B. *J. Am. Chem. Soc.* **1977**, *99*, 5525.
(2) Rice, S. F.; Milder, S. J.; Gray, H. B.; Goldbeck, R. A.; Kliger, D. S. *Coord. Chem. Rev.* **1982**, *43*, 349.
(3) Milder, S. J.; Kliger, D. S. *J. Phys. Chem.* **1985**, *89*, 4170.
(4) Milder, S. J.; Kliger, D. S.; Butler, L. G.; Gray, H. B. *J. Phys. Chem.* **1986**, *90*, 5567.
(5) Oberneder, S.; Gliemann, G. *J. Phys. Chem.* **1989**, *93*, 4487.
(6) Rice, S. F.; Gray, H. B. *J. Am. Chem. Soc.* **1981**, *103*, 1593.
(7) Rice, S. F.; Miskowski, V. M.; Gray, H. B. *Inorg. Chem.* **1988**, *27*, 4704.
(8) Marshall, J. L.; Stobart, S. R.; Gray, H. B. *J. Am. Chem. Soc.* **1984**, *106*, 3027.
(9) Winkler, J. R.; Marshall, J. L.; Netzel, T. L.; Gray, H. B. *J. Am. Chem. Soc.* **1986**, *108*, 2263.
(10) Gliemann, G.; Yersin, H. *Struct. Bonding* **1985**, *62*, 87 and references therein.
(11) Chassot, L.; Müller, E.; von Zelewsky, A. *Inorg. Chem.* **1984**, *23*, 4249.
(12) Bär, L.; Gliemann, G.; Chassot, L.; von Zelewsky, A. *Chem. Phys. Lett.* **1986**, *123*, 264.
(13) Pirzer, G.; Gliemann, G.; Chassot, L.; von Zelewsky, A. *Z. Naturforsch.* **1988**, *43A*, 983.
(14) Schindler, J. W.; Fukuda, R. C.; Adamson, A. W. *J. Am. Chem. Soc.* **1982**, *104*, 3596.
(15) Lechner, A.; Gliemann, G. *J. Am. Chem. Soc.*, in press.
(16) Zipp, A. P. *Coord. Chem. Rev.* **1988**, *84*, 47.
(17) Roundhill, D. M.; Gray, H. B.; Che, C.-M. *Acc. Chem. Res.* **1989**, *22*, 55.
(18) Sperline, R. P.; Dickson, M. K.; Roundhill, D. M. *J. Chem. Soc., Chem. Commun.* **1977**, 62.
(19) Fordyce, W. A.; Brummer, J. G.; Crosby, G. A. *J. Am. Chem. Soc.* **1981**, *103*, 7061.
(20) Parker, W. L.; Crosby, G. A. *Chem. Phys. Lett.* **1984**, *105*, 544.
(21) Dallinger, R. F.; Miskowski, V. M.; Gray, H. B.; Woodruff, W. M. *J. Am. Chem. Soc.* **1981**, *103*, 1595.
(22) Che, C.-M.; Butler, L. G.; Gray, H. B. *J. Am. Chem. Soc.* **1981**, *103*, 7796.
(23) Rice, S. F.; Gray, H. B. *J. Am. Chem. Soc.* **1983**, *105*, 4571.
(24) Che, C.-M.; Butler, L. G.; Gray, H. B.; Crooks, R. M.; Woodruff, W. H. *J. Am. Chem. Soc.* **1983**, *105*, 5492.
(25) Markert, J. T.; Clements, D. P.; Corson, M. R.; Nagle, J. K. *Chem. Phys. Lett.* **1983**, *97*, 175.
(26) Bär, L.; Gliemann, G. *Chem. Phys. Lett.* **1984**, *108*, 14.
(27) Vogler, A.; Kunkely, H. *Angew. Chem., Int. Ed. Engl.* **1984**, *12*, 316.
(28) Reisch, G. A.; Turner, W. A.; Corson, M. R.; Nagle, J. K. *Chem. Phys. Lett.* **1985**, *117*, 561.
(29) Stiegman, A. E.; Rice, S. F.; Gray, H. B.; Miskowski, V. M. *Inorg. Chem.* **1987**, *26*, 1112.
(30) Heuer, W. B.; Totten, M. D.; Rodman, G. S.; Hebert, E. J.; Tracy, H. J.; Nagle, J. K. *J. Am. Chem. Soc.* **1984**, *106*, 1163.
(31) Pinto, F. D. R.; Sadler, P. J.; Neidle, St.; Sanderson, M. R.; Subbiah, A.; Kuroda, R. *J. Chem. Soc., Chem. Commun.* **1980**, 13.
(32) Fetterolf, M.; Friedman, A. E.; Yang, Y.-Y.; Offen, H.; Ford, P. C. *J. Phys. Chem.* **1988**, *92*, 3760.

0020-1669/90/1329-1162$02.50/0

Table I. Crystal Data for $Ba_2[Pt_2(P_2O_5H_2)_4]\cdot 8H_2O$

M_r	1384.8	d_c, g·cm^{-3}	3.23
space group	*Pc*	d_o, g·cm^{-3}	>2.9
a, Å	9.5452 (8)	μ(Mo Kα), cm^{-1}	131.7
b, Å	19.459 (2)	radiation (monochromatized in incident beam	Mo Kα
c, Å	7.6611 (8)		
α, deg	90	*T*, K	295
β, deg	90.758 (8)	transm factors: max, min	1.0, 0.64
γ, deg	90	R_w(iso)	0.028
V, Å^3	1422.8	R_w(aniso)	0.027
Z	2	*w*	$1/\sigma^2(F)$

Table II. Positional Parameters and Their Estimated Standard Deviations for $Ba_2[Pt_2(P_2O_5H_2)_4]\cdot 8H_2O$[a]

atom	*x*	y	*z*	*B*, Å^2
Pt1	0.187**	0.26655 (2)	0.091**	0.814 (5)
Pt2	0.23737 (4)	0.23343 (2)	−0.27831 (5)	0.928 (5)
Ba1	0.71638 (7)	0.55895 (3)	0.66638 (8)	1.22 (1)
Ba2	0.71754 (7)	0.05892 (3)	0.64882 (8)	1.21 (1)
P1	0.0543 (3)	0.1692 (1)	0.1161 (3)	0.83 (4)
P2	0.3762 (3)	0.2012 (1)	0.1847 (4)	0.94 (4)
P3	0.3382 (3)	0.3640 (2)	0.0694 (4)	1.38 (5)
P4	0.0023 (3)	0.3322 (2)	0.0036 (4)	1.47 (5)
P5	0.1034 (3)	0.1375 (1)	−0.2504 (4)	1.03 (4)
P6	0.4317 (3)	0.1655 (2)	−0.1955 (4)	1.29 (4)
P7	0.3813 (3)	0.3296 (2)	0.6976 (4)	1.84 (5)
P8	0.0519 (3)	0.3007 (2)	−0.3698 (4)	1.68 (5)
O1	0.0930 (9)	0.1165 (5)	−0.042 (1)	1.6 (1)
O2	0.456 (1)	0.1658 (7)	0.014 (1)	4.8 (2)
O3	0.3508 (8)	0.3832 (4)	−0.139 (1)	1.6 (1)
O4	−0.0224 (9)	0.3305 (6)	−0.204 (1)	3.1 (2)
O11	−0.1067 (8)	0.1827 (4)	0.106 (1)	1.2 (1)*
O12	0.102 (1)	0.1213 (5)	0.271 (1)	2.3 (2)*
O21	0.352 (1)	0.1354 (5)	0.291 (1)	3.2 (2)*
O22	0.4904 (8)	0.2393 (4)	0.290 (1)	1.5 (1)*
O31	0.4966 (6)	0.3587 (4)	0.134 (1)	1.2 (1)*
O32	0.267 (1)	0.4338 (5)	0.123 (1)	2.2 (2)*
O41	0.0020 (9)	0.4084 (5)	0.051 (1)	2.1 (2)*
O42	−0.1382 (8)	0.3019 (6)	0.082 (1)	2.3 (2)*
O51	−0.0335 (7)	0.1381 (5)	−0.321 (1)	1.4 (1)*
O52	0.1658 (8)	0.0698 (4)	−0.337 (1)	1.2 (1)*
O61	0.430 (1)	0.0896 (4)	−0.242 (1)	2.7 (2)*
O62	0.5876 (8)	0.1886 (4)	−0.245 (1)	1.8 (1)*
O71	0.536 (1)	0.3264 (5)	0.686 (1)	1.8 (2)*
O72	0.3535 (8)	0.3763 (4)	0.5307 (9)	1.2 (1)*
O81	0.0820 (8)	0.3575 (4)	−0.495 (1)	1.5 (1)*
O82	−0.0779 (9)	0.2565 (5)	−0.444 (1)	2.5 (1)*
O91	−0.2726 (8)	0.4204 (4)	−0.200 (1)	1.4 (1)*
O92	0.513 (1)	0.4850 (5)	0.414 (1)	1.8 (2)*
O93	−0.1028 (8)	0.4672 (4)	0.454 (1)	1.2 (1)*
O94	0.7190 (9)	0.3374 (5)	0.405 (1)	1.9 (1)*
O95	0.523 (1)	0.0288 (6)	0.384 (1)	2.5 (2)*
O96	−0.0896 (9)	0.0161 (4)	0.373 (1)	1.4 (1)*
O97	0.713 (1)	0.0804 (5)	0.025 (1)	2.1 (2)*
O98	−0.2727 (9)	0.1544 (4)	0.391 (1)	1.7 (1)*

[a] Starred values are for atoms that were refined isotropically. *B* values for anisotropically refined atoms are given in the form of the isotropic equivalent thermal parameter defined as $^4/_3[a^2B(1,1) + b^2B(2,2) + c^2B(3,3) + ab(\cos\gamma)B(1,2) + ac(\cos\beta)B(1,3) + bc(\cos\alpha)B(2,3)]$. Two stars indicate a fixed position.

reported. The purpose of this study is to find out (i) if in the crystal the binuclear units can be pushed together, yielding an intercomplex coupling of neighboring Pt–Pt pairs and (ii) if this process depends on variations of the crystal structure.

Experimental Section

$Ba_2[Pt_2(P_2O_5H_2)_4]$ was prepared by the method of Rice and Gray.[23] For $(NH_4)_4[Pt_2(P_2O_5H_2)_4]$ a correspondingly modified method described by Pinto et al.[31] for the potassium compound has been applied. Yellow-green single crystals of the compounds have been obtained from aqueous solutions. The crystals showed dichroism in transmission. Whereas the Ba–POP crystals have been proved to be stable at normal conditions, the surface of NH_4–POP crystals is very sensitive to moisture. For this reason NH_4–POP crystals have been protected by a thin paraffin coating.

Table III. Selected Bond Distances (in Å) for $Ba_2[Pt_2(P_2O_5H_2)_4]\cdot 8H_2O$

Pt1–Pt2	2.949 (0)	P6–O62	1.605 (8)
Pt1–P1	2.288 (5)	P7–O3	1.66 (2)
Pt1–P2	2.314 (5)	P7–O71	1.480 (11)
Pt1–P3	2.391 (5)	P7–O72	1.588 (9)
Pt1–P4	2.270 (6)	P8–O4	1.573 (15)
Pt2–P5	2.274 (5)	P8–O81	1.493 (9)
Pt2–P6	2.357 (5)	P8–O82	1.606 (8)
Pt2–P7	2.330 (6)	Ba1–O41	2.944 (7)
Pt2–P8	2.304 (5)	Ba1–O42	3.114 (6)
P1–O1	1.633 (14)	Ba1–O91	2.885 (13)
P1–O11	1.560 (10)	Ba1–O91	2.837 (11)
P1–O12	1.568 (9)	Ba1–O92	3.077 (9)
P2–O2	1.67 (2)	Ba1–O92	2.864 (10)
P2–O21	1.538 (9)	Ba1–O93	2.980 (8)
P2–O22	1.539 (7)	Ba1–O93	2.828 (8)
P3–O3	1.646 (14)	Ba1–O94	2.720 (9)
P3–O31	1.588 (9)	Ba2–O51	2.839 (8)
P3–O32	1.576 (10)	Ba2–O61	2.938 (7)
P4–O4	1.605 (15)	Ba2–O62	2.932 (7)
P4–O41	1.528 (9)	Ba2–O95	2.790 (9)
P4–O42	1.589 (8)	Ba2–O95	3.112 (9)
P5–O1	1.652 (14)	Ba2–O96	2.943 (7)
P5–O51	1.406 (8)	Ba2–O96	2.894 (7)
P5–O52	1.593 (9)	Ba2–O97	2.911 (11)
P6–O2	1.62 (2)	Ba2–O97	2.874 (11)
P6–O61	1.521 (9)	Ba2–O98	2.711 (8)

The high-pressure experiments were performed by a special spectrometer with a modified sapphire cell of Bridgman's opposed anvil type.[34,35] The pressure within the cell was determined by the pressure shift of the *R* lines (−0.76 cm^{-1}/kbar at $\sim$3 K $\leq T \leq$ 298 K) of small ruby crystals.[36] For measurements at low temperatures, the cell was positioned inside a helium Dewar flask. As excitation source for the emission, the 364-nm line of an argon ion laser (Type 165, Spectra Physics) was used. The emission light was analyzed by a Spex single-grating monochromator (Type 1700) and an EMI S20 photomultiplier.

For the magnetooptical measurements a superconducting magnet of Oxford Instruments (SM4) yielding magnetic fields up to 6 T has been used. Excitation was by the 364-nm line of a Coherent argon ion laser. The emitted light was selected by a Spex double-grating monochromator (Type 1404) and detected by an EMI S20 photomultiplier.

A single crystal of $Ba_2[Pt_2(P_2O_5H_2)_4]\cdot 8H_2O$ (approximate dimensions 0.25 × 0.15 × 0.08 mm^3) was used for data collection on an Enraf-Nonius CAD-4 diffractometer (Mo Kα, λ = 0.71073 Å, graphite monochromator in incident beam). The lattice constants were refined from 2θ values of 25 reflections in the range $8.1 \leq \theta \leq 17.3°$. Intensities were measured for $2 \leq \theta \leq 30°$ in an ω–2θ-scan technique, scan width $(1.25 + 0.35 \tan\theta)°$. An experimental correction of the serious absorption effects was applied, based on ψ scans; transmission factors varied between 64.1 and 99.7%. Three standard reflections indicated an intensity loss of 2.6% throughout data collection. Merging of the 4637 collected intensities ($(\sin\theta_{max})/\lambda$ = 0.71 Å^{-1}; $-10 \leq h \leq 10$, $0 \leq k \leq 27$, $0 \leq l \leq 13$) gave 4267 unique reflections (R_{int} = 0.009), of which 3284 with $I > 3\sigma(I)$ were considered as observed and used for all calculations (program system SDP 3.0; Enraf-Nonius).

Because there was no sufficient material for a pycnometric density determination, we could only show that the density of a crystal fragment was higher than that of bromoform (d = 2.9 g·cm^{-3}). This agrees with Z = 2 (d_c = 3.23 g·cm^{-3}), a value which was confirmed by the structure refinement.

The structure was solved by Patterson and routine direct methods using the SDP program. Systematic absences from the data indicated that the space group was either $P2/c$ or *Pc*. A $N(Z)$ test suggested an acentric structure, and the space group *Pc* was selected and later proved to be correct by the successful refinement.

In full-matrix least-squares refinement $|F|$ magnitudes were used to refine atomic coordinates and temperature factors of the non-hydrogen atoms (anisotropic for Pt, Ba, P, and O1–O4; isotropic for O11–O98). Final R = 0.021, R_w = 0.027, $w^{-1} = \sigma^2(F)$, maximum Δ/σ = 2.1 in final

(33) Stroud, M. A.; Drickamer, H. G.; Zietlow, M. H.; Gray, H. B.; Swanson, B. I. *J. Am. Chem. Soc.* **1989**, *111*, 66.

(34) Weis, C. E.; Piermarini, G. J.; Block, S. *Rev. Sci. Instrum.* **1969**, *40*, 1133.

(35) Barnett, J. P.; Block, S.; Piermarini, G. J. *Rev. Sci. Instrum.* **1973**, *44*, 1.

(36) Noack, R. A.; Holzapfel, W. B. *High Pressure Science and Technology*; Plenum Press: New York, 1979; Vol. 1.

Table IV. Selected Bond Angles (in deg) for $Ba_2[Pt_2(P_2O_5H_2)_4]\cdot 8H_2O$

Pt2-Pt1-P1	89.8 (1)	O11-P1-O12	114.3 (5)
Pt2-Pt1-P2	92.3 (1)	O2-P2-O21	98.4 (9)
Pt2-Pt1-P3	90.0 (1)	O2-P2-O22	106.4 (9)
Pt2-Pt1-P4	88.6 (1)	O21-P2-O22	103.5 (4)
P1-Pt1-P2	87.1 (2)	O3-P3-O31	103.7 (6)
P1-Pt1-P3	176.4 (2)	O3-P3-O32	95.5 (7)
P1-Pt1-P4	93.6 (2)	O31-P3-O32	112.8 (5)
P2-Pt1-P3	89.3 (2)	O4-P4-O41	105 (1)
P2-Pt1-P4	178.9 (2)	O4-P4-O42	104.6 (8)
P3-Pt1-P4	90.0 (2)	O41-P4-O42	105.3 (5)
Pt1-Pt2-P5	89.4 (1)	O1-P5-O51	107.7 (6)
Pt1-Pt2-P6	90.1 (1)	O1-P5-O52	103.0 (7)
Pt1-Pt2-P7	90.3 (1)	O51-P5-O52	101.4 (5)
Pt1-Pt2-P8	91.9 (1)	O2-P6-O61	104 (1)
P5-Pt2-P6	87.5 (2)	O2-P6-O62	96.4 (9)
P5-Pt2-P7	177.9 (2)	O61-P6-O62	102.8 (5)
P5-Pt2-P8	93.7 (2)	O3-P7-O71	104.9 (6)
P6-Pt2-P7	90.5 (2)	O3-P7-O72	102.6 (6)
P6-Pt2-P8	177.7 (2)	O71-P7-O72	97.5 (5)
P7-Pt2-P8	88.4 (2)	O4-P8-O81	109.7 (9)
O1-P1-O11	107.5 (6)	O4-P8-O82	97.4 (9)
O1-P1-O12	97.0 (6)	O81-P8-O82	108.9 (5)

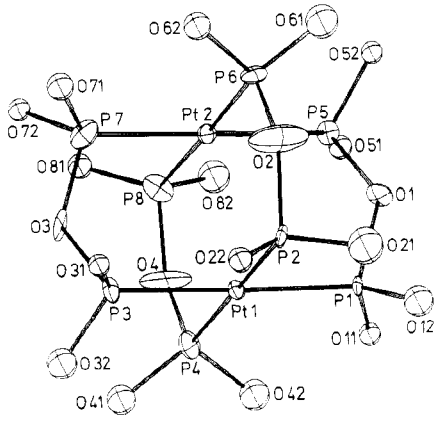

Figure 1. ORTEP plot of the anion $[Pt_2(P_2O_5H_2)_4]^{4-}$.

refinement cycle with 321 parameters, and $S = 2.8$. The maximum features in the $\Delta\rho$ map are +1.4 and −0.85 e Å^{-3}.

Results

Structure. The space group of the $Ba_2[Pt_2(P_2O_5H_2)_4]\cdot 8H_2O$ crystal is *Pc* with $Z = 2$ and lattice constants $a = 9.5452$ (8) Å, $b = 19.459$ (2) Å, $c = 7.6611$ (8) Å, and $\beta = 90.758$ (8)°. Additional crystal data can be taken from Table I. Atomic coordinates are listed in Table II; selected bond distances and angles, in Tables III and IV, respectively.

The anion consists of two Pt atoms 2.949 Å apart; cf. Figure 1. Each Pt is surrounded by a slightly distorted square of four P atoms. The P atoms are joined by oxygen (O1–O4). O11–O82 include the two nonbridging oxygens on each P. The atoms O91–O98 belong to the water molecules.

The anions form two sets of parallel chains; cf. Figure 2. In each chain the Pt–Pt axes are parallel, forming an angle of about 16° with the chain axis (crystallographic *z* axis). Adjacent Pt atoms of neighboring anions of a chain are 4.90 Å apart. The Pt–Pt axes of anions in chains of different sets form an angle of 25.4°. Between the chains are the cations. Each Ba atom is surrounded by 10 oxygen atoms, 3 of which are part of the diphosphito groups and 7 belong to water molecules.

Luminescence at Different Temperatures and Magnetic Fields. Between $T = 1.9$ K and room temperature and at ambient pressure single crystals of NH_4–POP and Ba–POP show a bright luminescence. The emission spectrum of each compound is composed of a phosphorescence band P and a fluorescence band F, which differ distinctly by their spectral position and their lifetime, as shown in Table V.

At $T \lesssim 4.2$ K the fluorescence bands F of NH_4–POP and Ba–POP have a pronounced fine structure and exhibit a polarization ratio $I_\parallel/I_\perp$ of about 10, with $I_\parallel$ and $I_\perp$ the integral intensity of the $\mathbf{E}\parallel\mathbf{z}$- and $\mathbf{E}\perp\mathbf{z}$-polarized fluorescence, respectively. The fine structure is formed by a progression of $\sim 114 \pm 2$ cm^{-1}, and each line of the progression has a satellite red shifted by ~40–50 cm^{-1}. These satellites are more intense for Ba–POP than for NH_4–POP. With increasing temperature the fine structure of the fluorescence bands obscures, and at $T = 70$ K it disappears; the spectral positions of the bands, however, remain constant in this temperature range. Between $T = 70$ and 200 K the maxima of the fluorescence bands are red shifted by ~4 cm^{-1}/K. For both compounds the fluorescence intensity grows by a factor of about 2, if the temperature is increased from $T = 10$ to 100 K. Further temperature increase lowers the intensity drastically.

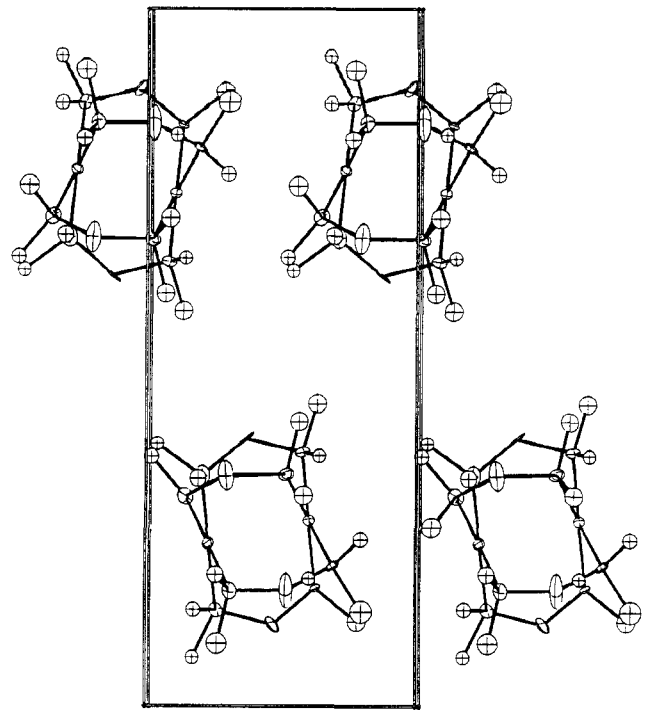

Figure 2. ORTEP plot of the anions $[Pt_2(P_2O_5H_2)_4]^{4-}$ in the $Ba_2[Pt_2(P_2O_5H_2)_4]\cdot 8H_2O$ crystal. Projection is on (100).

Table V. Energies and Decay Times of the Fluorescence and of the Phosphorescence at $T = 4.2$ K[a]

	fluorescence		phosphorescence	
compd	$\bar{\nu}_{max}$, cm^{-1}	τ, ns	$\bar{\nu}_{max}$, cm^{-1}	τ, ms
NH_4–POP	24 850	<2	19 140	10
	(24 330)	(<2)	(19 380)	(0.01)
Ba–POP	25 350	<2	19 530	10
	(24 830)	(<2)	(19 820)	(0.01)

[a] The values in parentheses are for $T = 200$ K.

For single crystals NH_4–POP and Ba–POP at $1.9 \text{ K} \le T \le 10$ K, neither the energy of the fine structure lines nor the intensity of the fluorescence can be influenced by magnetic fields with $0 \le H \le 5$ T.

At low temperatures ($T \lesssim 4.2$ K) the phosphorescence bands are weakly $\mathbf{E}\parallel\mathbf{z}$ polarized with a polarization ratio of ~1.4 (NH_4–POP) and ~2.0 (Ba–POP), respectively; cf. Figure 3. The phosphorescence band of Ba–POP exhibits a weak fine structure composed of two 112-cm^{-1} progressions superimposed on a broad basis band. At the high-energy side of the NH_4–POP band the fine structure is more pronounced, indicating a progression of ~115 cm^{-1}. The maximum of the basis band of NH_4–POP, defined as the maximum of the curve that connects the minima between the fine-structure peaks, has the energy $\bar{\nu} = 19\,140$ cm^{-1}. The wavenumber of the corresponding maximum of the Ba–POP spectrum is $\bar{\nu} = 19\,530$ cm^{-1}.

Variation of the temperature between $T = 1.9$ and 4.2 K yields no change of the phosphorescence spectra. With increase of temperature to $T = 10$ K the maxima of the phosphorescence bands are shifted to higher energies by $\Delta\bar{\nu} \sim 240 \pm 20$ cm^{-1} for

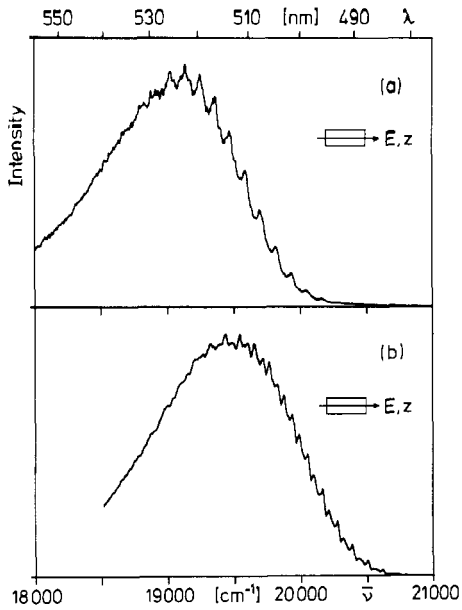

Figure 3. Phosphorescence spectra of single-crystal $(NH_4)_4[Pt_2(POP)_4]$ at $T = 4.2$ K (a) and $Ba_2[Pt_2(POP)_4]$ at $T = 1.7$ K (b). $\lambda_{exc} = 364$ nm.

NH_4–POP, cf. Figure 4b, and by $\Delta\bar{\nu} \sim 320 \pm 20$ cm^{-1} for Ba–POP, and fine structures grow up exhibiting distinct progressions of 115 cm^{-1} (for NH_4–POP) and 112 cm^{-1} (for Ba–POP). The lines constituting the fine structures have a half-width of about 20 cm^{-1}, and each of these lines is provided with a weak satellite red shifted by ~40 cm^{-1}. At the low-energy range the lines are accompanied by one additional very weak satellite each, which is red shifted by ~80 cm^{-1} from the corresponding line maximum. With further temperature increase to $T = 70$ K the fine structures become more and more indistinct; however, the energies of the lines remain constant within a limit of $\Delta\bar{\nu} = \pm 10$ cm^{-1} and no shift of the phosphorescence maxima has been detected. At $T \gtrsim 10$ K the phosphorescence of both compounds is predominantly $\mathbf{E} \perp \mathbf{z}$ polarized ($I_\perp/I_\parallel \sim 4$).

With a homogeneous magnetic field $\mathbf{H} \perp \mathbf{z}$ at $T = 4.2$ K an increase of the magnetic field strength from $H = 0$ to 4 T intensifies the phosphorescence by a factor of ~2 and shifts the basis bands to the blue by $\Delta\bar{\nu} \sim 200 \pm 20$ cm^{-1} (NH_4–POP), cf. Figure 4c, and respectively by $\Delta\bar{\nu} \sim 280 \pm 20$ cm^{-1} (Ba–POP). Simultaneously distinct fine structures grow up, which exhibit the same progressions as in the corresponding zero-field spectra at $T = 10$ K, but they are red shifted by 41 ± 2 cm^{-1}. At 4 T $\leq H \leq 6$ T no additional magnetic field effect on the phosphorescence could be observed.

The magnetic field effect depends distinctly on the temperature. With increasing temperature the intensity of the described magnetic field induced progression (at $T = 4.2$ K) competes with the intensity of the progression observed at $T = 10$ K and zero field, as shown in Figure 4d for NH_4–POP. At $T > 20$ K only the temperature-induced progression (10 K progression at zero field) can be detected, independent of the magnetic field strength $H \leq 6$ T.

For single-crystal Ba–POP the magnetic field effects are nearly independent of the orientation of the magnetic field **H**. For NH_4–POP, however, the magnetic field induced progression at $T = 10$ K has maximum intensity if **H** is perpendicular to the crystallographic z axis.

Luminescence at High Pressures. Figures 5 and 6 show the room-temperature luminescence spectra of single-crystal NH_4–POP and Ba–POP, respectively, at different pressures. At ambient pressure each compound exhibits a phosphorescence band P and a fluorescence band F. The bands F are red shifted by ~500 cm^{-1} between $p = 1$ bar and ~15 kbar, and they disappear when the pressure is increased to $p \gtrsim 20$ kbar. The phosphorescence bands P of both compounds manifest very different features with increasing pressure. For Ba–POP the band P is red shifted from $\bar{\nu} = 19\,800$ to $19\,050$ cm^{-1} and its half-width is increased from

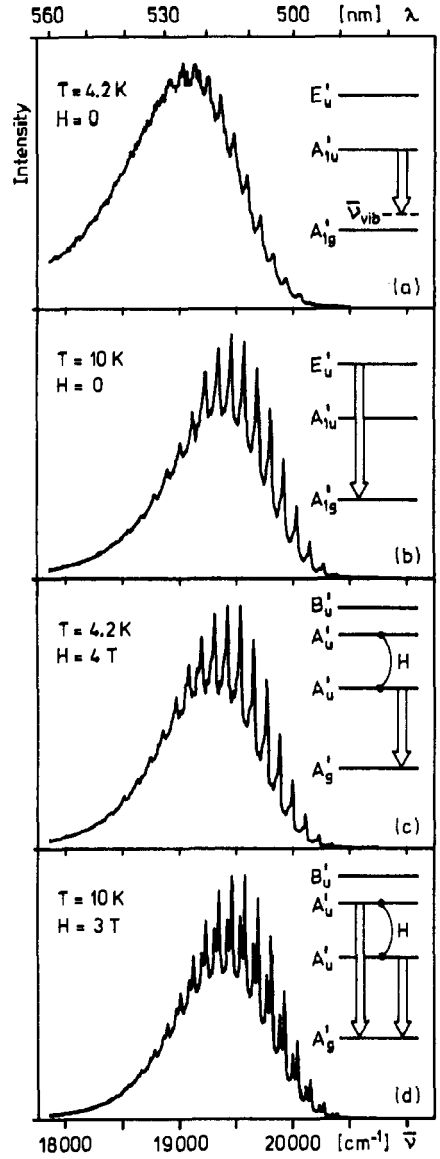

Figure 4. Phosphorescence spectra of single-crystal $(NH_4)_4[Pt_2(POP)_4]$ at different magnetic field strengths and different temperatures ($\mathbf{H} \perp \mathbf{z}$, $\mathbf{E} \perp \mathbf{z}$; $\lambda_{exc} = 364$ nm): (a) $T = 4.2$ K, $H = 0$; (b) $T = 10$ K, $H = 0$; (c) $T = 4.2$ K, $H = 4$ T; (d) $T = 10$ K, $H = 3$ T. The inserts show schematically the corresponding optical transitions and the involved spin–orbit states.

$\Delta\bar{\nu}_{1/2} \sim 1600$ to 2800 cm^{-1} if the pressure is raised from $p = 1$ bar to 30 kbar. Within this pressure range the intensity of the Ba–POP phosphorescence is reduced by a factor of about 20. For NH_4–POP a pressure-induced red shift of the phosphorescence band P could not be recognized definitely, since with increasing pressure an additional band D grows up at the red flank of band P and dominates the phosphorescence at $p \gtrsim 5$ kbar. In the pressure range 10 kbar $\lesssim p \lesssim 40$ kbar, band D shows a red shift of $\Delta\bar{\nu}/\Delta p \sim -10$ cm^{-1}/kbar; cf. Figure 7. With increasing pressure the intensities of both band P and D are strongly reduced. Between $p = 1$ bar and ~15 kbar this reduction is more intense for band P than for band D; at $p > 15$ kbar the intensity decrease of band D surpasses that of band P.

At low temperatures ($T \lesssim 10$ K) control measurements at ruby crystals differently positioned inside the sample chamber have shown that the pressure profile in the pressure cell was not isotropic. Maximum differences of $\Delta p \sim \pm 5$ kbar have been found. This effect is probably due to a temperature-induced enhancement of the viscosity of the paraffin, which has been used as transmission medium for the pressure. Thus, the values of the applied pressure determined at low temperatures are correspondingly uncertain.

Figure 8 shows the 10 K phosphorescence spectra of NH_4–POP at different pressures. With increasing pressure the fine structure

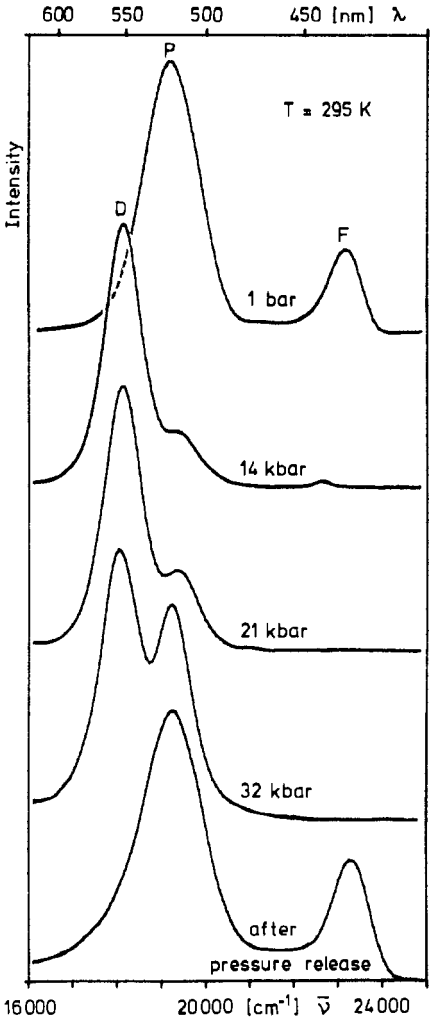

Figure 5. Emission spectra of single-crystal $(NH_4)_4[Pt_2(POP)_4]$ at different pressures. T = 295 K; λ_{exc} = 364 nm. The intensities at different pressures are not comparable.

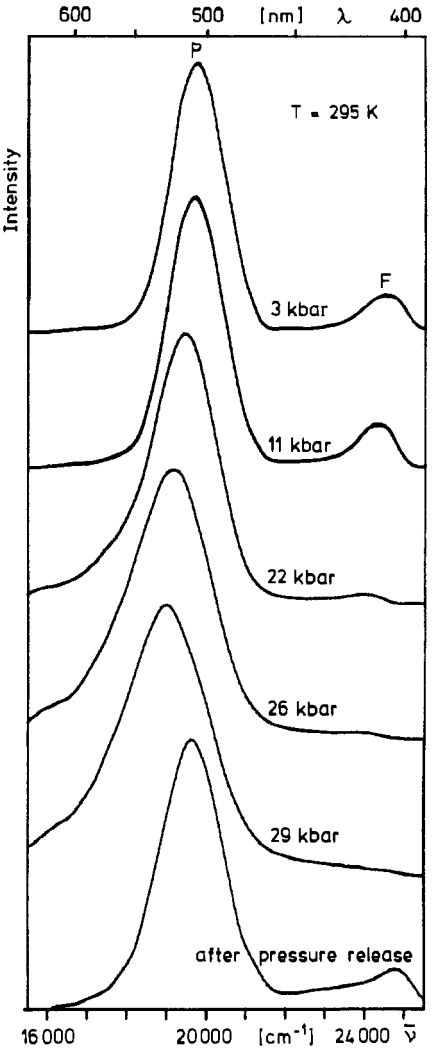

Figure 6. Emission spectra of single-crystal $Ba_2[Pt_2(POP)_4]$ at different pressures. T = 295 K; λ_{exc} = 364 nm. The intensities at different pressures are not comparable.

of the phosphorescence band P becomes indistinct and the maximum of P is red shifted by $\Delta\nu/\Delta p \sim (-6 \pm 2)$ cm^{-1}/kbar; within the limit of the strongly decreasing detectibility the vibrational spacing is not changed. At $p \sim 30$ kbar an additional band D occurs at the red flank of band P. This band D shows a pressure-induced red shift slightly larger than that of band P, and at high pressures band D dominates the emission.

The luminescence spectrum of single-crystal Ba–POP at T = 10 K is also influenced by applied pressure. As for NH_4–POP the fine structure of the phosphorescence band P disappears if the pressure is increased; however, no additional band of type D occurs. Only a red shift of band P and of the fluorescence band F has been observed, as summarized in Figure 9. The red shift of band F, $\Delta\bar{\nu}/\Delta p \sim -25$ cm^{-1}/kbar, is by a factor of $\sim$2.5 larger than that of band P. At T = 1.7 K the red shift of band P is reduced to $\Delta\bar{\nu}/\Delta p \sim -5$ cm^{-1}/kbar.

The pressure-induced changes of the luminescence spectra are reversible within the limits of experimental error. Reduction of the pressure to p = 1 bar (and temporary heating of the samples used in the low temperature experiments for $t \gtrsim 12$ h to $T \sim 100$ K) yields the original spectra; cf. the examples shown in Figures 5 and 6.

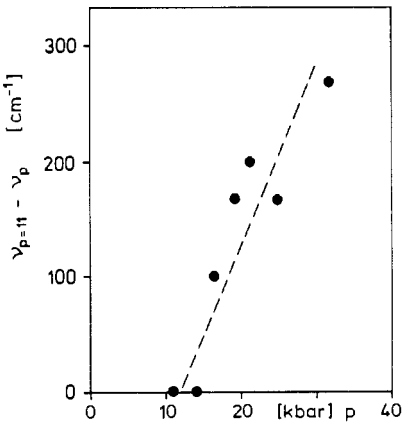

Figure 7. Red shift of the pressure-induced emission band D of single-crystal $(NH_4)_4[Pt_2(POP)_4]$ as a function of pressure. T = 295 K; λ_{exc} = 364 nm.

Discussion

The $[Pt_2(POP)_4]^{4-}$ complex ions have nearly D_{4h} point symmetry with the Pt–Pt axis **c** as the 4-fold symmetry axis. The HOMO and the LUMO of the complex ion can be assigned to the orbitals $\sigma^*(5d_{z^2})$ and $\sigma(6p_z)$, respectively, of the binuclear metal d^8–d^8 system.[19] If spin–orbit coupling (double group D_{4h}') is taken into account, the ground electronic state has the symmetry $A_{1g}'(^1A_{1g})$ and the lowest excited states transform according to $A_{2u}'(^1A_{2u})$ and $A_{1u}', E_u'(^3A_{2u})$. The singlet–singlet transition $A_{2u}' \rightarrow A_{1g}'$ is electric dipole allowed with polarization $\mathbf{E} \| \mathbf{c}$ and manifests itself as the fluorescence. The phosphorescence is due to the radiative deactivation of the triplet components A_{1u}' and E_u'. Whereas the $\mathbf{E} \perp \mathbf{c}$-polarized transition $E_u' \rightarrow A_{1g}'$ acquires intensity by an admixture of the excited singlet ^1E_u (excited configurations $[\pi^*(5d_{xz},5d_{yz})]^3[\sigma^*(6p_z)]^1$ and $[\pi(5d_{xz},5d_{yz})]^3[\sigma(6p_z)]^1$; cf. ref 37)

(37) Isci, H.; Mason, W. R. *Inorg. Chem.* **1985**, *24*, 1761.

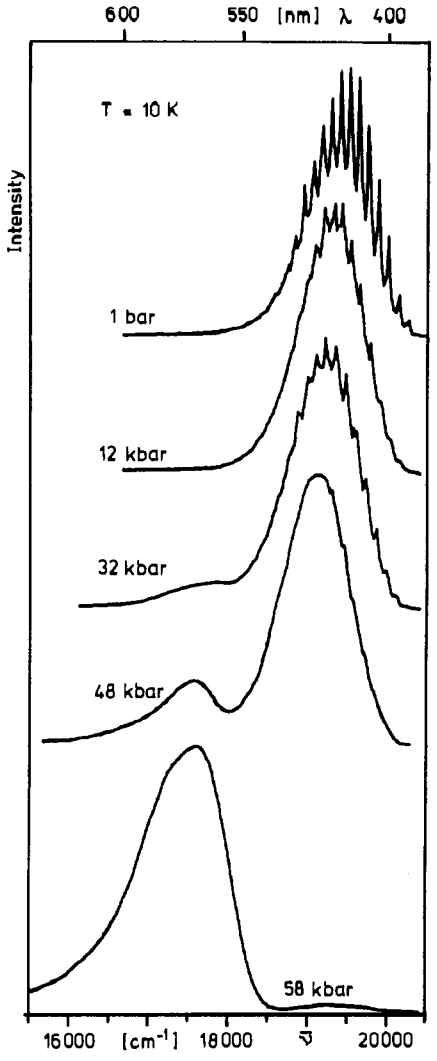

Figure 8. Emission spectra of single-crystal $(NH_4)_4[Pt_2(POP)_4]$ at different pressures. T = 10 K; λ_{exc} = 364 nm. The intensities at different pressures are not comparable.

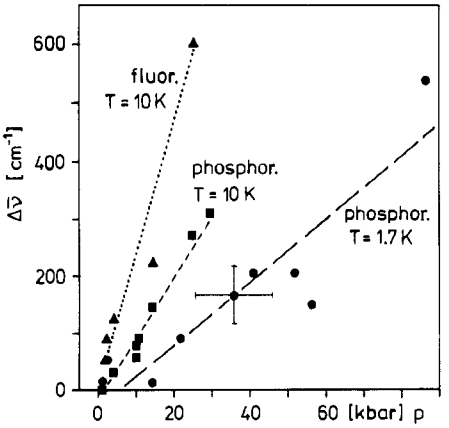

Figure 9. Red shifts of the emission maxima of single-crystal $Ba_2Pt_2(POP)_4$ as functions of pressure. T = 1.7 and 10 K.

to E_u', the transition $A_{1u}' \rightarrow A_{1g}'$ is symmetry- and spin-forbidden. The phosphorescence from the state A_{1u}' can be activated by vibronic coupling with e_g and a_{2g} vibrations, yielding the vibronic transitions $A_{1u}' \rightarrow A_{1g}' + e_g$ ($\mathbf{E} \perp \mathbf{c}$) and $A_{1u}' \rightarrow A_{1g}' + a_{2g}$ ($\mathbf{E} \parallel \mathbf{c}$), respectively.

As shown above, in single-crystal Ba–POP the molecular **c** axes (Pt–Pt axes) are inclined toward the crystallographic z axis by angles of ~16°. Therefore, both experimental polarizations $\mathbf{E} \parallel \mathbf{z}$ and $\mathbf{E} \perp \mathbf{z}$ are corresponding superpositions of the polarizations $\mathbf{E} \parallel \mathbf{c}$ and $\mathbf{E} \perp \mathbf{c}$. For single-crystal NH_4–POP no structure data are available. However, as will be shown below, the luminescence properties of this system can be understood, if in the crystal all molecular **c** axes (Pt–Pt axes) are parallel with the crystallographic z axis, a structural feature that has been found for the potassium compound $K_4[Pt_2(POP)_4]$.[31]

Differences of the electronic spectra of the barium and the ammonium compound can be traced back to structural differences. At $T \leq 4.2$ K both the fluorescence and the phosphorescence of Ba–POP have energies higher by ~500 cm^{-1} and ~390 cm^{-1}, respectively, than the corresponding emission bands of NH_4–POP. Since with decreasing Pt–Pt distance, R, the energy gap between the HOMO and the LUMO decreases, for NH_4–POP a smaller R value than that for the barium compound is expected, $R(NH_4) < R(Ba) = 2.949$ Å. A comparison with the corresponding properties of the potassium compound confirms this correlation. K–POP shows a phosphorescence at $\bar{\nu} = 19\,100$ cm^{-1} and has a Pt–Pt distance of $R(K) = 2.925$ Å.[31]

The assignment of the transitions that give rise to the highly structured fluorescence and phosphorescence spectra of the $[Pt_2(POP)_4]^{4-}$ complex ion at normal pressure and at zero magnetic field has been discussed comprehensively.[19-26] Here, only several conspicuous features of the phosphorescence spectra of single-crystal Ba–POP and NH_4–POP will be analyzed. From the intensity ratio $I_\parallel/I_\perp \sim 2$ and the emission lifetimes of both compounds at 1.7 K $\leq T \leq$ 4.2 K, it can be concluded that the low-temperature phosphorescence is due to vibronic transitions from the state A_{1u}' assisted by e_g and a_{2g} vibrations. The progressions of the fine-structure lines originate from the Pt–Pt stretching vibration.[38,39] The vibrational interval for NH_4–POP ($\Delta\bar{\nu} \sim 115$ cm^{-1}) is slightly larger than that for Ba–POP ($\Delta\bar{\nu} \sim 112$ cm^{-1}), which may be due to the different Pt–Pt distances, $R(NH_4) < R(Ba)$. Until now the origin of the red-shifted satellites of the fine-structure lines is not explained definitely. Rice and Gray[23] have assigned these satellites to quanta of a low-energy totally symmetric vibration (probably a ligand deformation) superimposed on the main lines of the progression. Recently, Ikeyama et al.[40] have attributed the satellites to $[Pt_2(POP)_4]^{4-}$ ions at different sites. The latter interpretation seems to be unlikely, since single crystals differently prepared and with different cations yield very similar fine structures. From a Franck–Condon analysis of the phosphorescence spectrum of K–POP, Ikeyama et al. have detected an additional broad-banded progression that is responsible for the broad basis of the spectrum. A similar progression inhomogeneously broadened by different sites (of slightly disordered complex ions) is probably due also to the broad shapes of the spectra of Ba–POP and NH_4–POP.

With increase of the temperature to $T \sim 10$ K the triplet component $E_u'(^3A_{2u})$ is thermally occupied and the allowed $\mathbf{E} \perp \mathbf{z}$-polarized transition $E_u' \rightarrow A_{1g}'$ dominates the phosphorescence; cf. Figure 4b. By that means the $\mathbf{E} \perp \mathbf{z}$-polarized phosphorescence is blue shifted by $\Delta\bar{\nu} = \Delta E + \bar{\nu}(e_g)$, with ΔE the energy gap between E_u' and A_{1u}' and $\bar{\nu}(e_g)$ the quantum of an e_g vibration, and the polarization ratio $I_\parallel/I_\perp$ is decreased from ~2 to ~0.25.

The magnetic field effect on the phosphorescence will be discussed for single-crystal NH_4–POP with orientations $\mathbf{H} \perp \mathbf{z}$, $\mathbf{E} \perp \mathbf{z}$; cf. Figure 4c,d. A homogeneous magnetic field $\mathbf{H} \perp \mathbf{c}$ reduces the symmetry of the molecular system from D_{4h}' to C_{2h}'. Then the upper triplet component E_u' splits into the nondegenerate states B_u' and A_u'. The latter can mix with the lower triplet component $A_u'(A_{1u}')$, and thus, a new radiative $\mathbf{E} \perp \mathbf{c}$-polarized channel from the lowest A_u' to the vibrationally nonexcited electronic ground state $A_g'(A_{1g}')$ is opened. Its energy is larger by the vibration quantum $\bar{\nu}(e_g)$ than that of the low-temperature phosphorescence at zero field. At low temperature (cf. Figure 4c) this new transition competes with the low-energy vibronic transition as the magnetic field strength H increases, yielding (i) a corresponding blue shift $\Delta\bar{\nu} \leq \bar{\nu}(e_g)$ of the phosphorescence and (ii) an increase of the intensity.[26,28] The experimental values $\Delta\bar{\nu} \sim 200 \pm 20$ cm^{-1}

(38) Kurmoo, M.; Clark, R. J. H. *Inorg. Chem.* **1985**, *24*, 4420.
(39) Stein, P.; Dickson, M. K.; Roundhill, D. M. *J. Am. Chem. Soc.* **1983**, *105*, 3489.
(40) Ikeyama, T.; Yamamoto, S.; Azumi, T. *J. Phys. Chem.* **1988**, *92*, 6899.

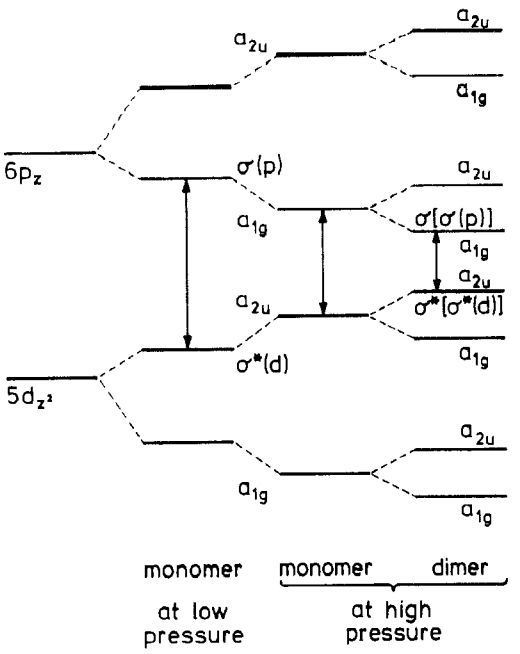

Figure 10. MO diagrams of the monomer $[Pt_2(POP)_4]^{4-}$ and of the dimer $\{[Pt_2(POP)_4]^{4-}\}_2$ schematic. The arrows connect the HOMO and the LUMO in each system, respectively.

(NH_4–POP) and $\Delta\bar{\nu} \sim 280 \pm 20$ cm^{-1} (Ba–POP) at $H = 4$ T have to be compared with e_g vibrational quantums of the systems. Vibrations with 232, 241, 278, and 308 cm^{-1} have been reported by Roundhill et al.,[39] but no symmetry assignment of these vibrations is available until now.

At $T \geq 10$ K and $H \neq 0$ both the radiative deactivation of the thermally occupied states A_u', $B_u'(E_u')$ and the emission via the magnetic field induced channel $A_u'(A_{1u}') \rightarrow A_g'$ are allowed; cf. Figure 4d. The energies of the two transitions differ by ΔE, provided the energy of the splitting of E_u' can be neglected. Since the phosphorescence spectrum of each compound is a superposition of the two mentioned emission spectra, the spacing of two equivalent fine-structure lines corresponds to the energy difference between the triplet components $A_u'(E_u')$ and $A_u'(A_{1u}')$. Our experimental value $\Delta E = 41 \pm 2$ cm^{-1} found for Ba–POP and NH_4–POP is in agreement with the ΔE value determined by Nagle et al.[25] for K–POP.

The different sensitivity of the phosphorescence of single-crystal Ba–POP and NH_4–POP to the orientation of the magnetic field **H** can be traced back to their different crystal structures. For $\mathbf{E} \perp \mathbf{c}$ polarization only fields with orientation $\mathbf{H} \perp \mathbf{c}$ yield the effect described above. In single-crystal Ba–POP all Pt–Pt axes **c** are inclined to the crystallographic axis *z* and, thus, the magnetic field is effective for both orientations $\mathbf{H} \perp \mathbf{z}$ and $\mathbf{H} \parallel \mathbf{z}$, since in every case a nonvanishing component $\mathbf{H} \perp \mathbf{c}$ exists. For NH_4–POP, however, the **c** axes are assumed to be parallel to the crystallographic *z* axis. Thus, $\mathbf{H} \perp \mathbf{z}$ and $\mathbf{H} \parallel \mathbf{z}$ are equivalent to $\mathbf{H} \perp \mathbf{c}$ and $\mathbf{H} \parallel \mathbf{c}$, respectively.

By high pressure the luminescence of single-crystal $M_x[Pt_2(POP)_4]$ can be affected in different ways; all are mainly due to changes of the Pt–Pt distances as a consequence of the compression of the crystal. Two of the resulting features are particularly pronounced for the ammonium compound.

One effect is the pressure-induced reduction ΔR of the intracomplex Pt–Pt distance *R*. By that means the energy gap between the HOMO and the LUMO of the single $[Pt_2(POP)_4]^{4-}$ ion decreases and the corresponding low-energy electronic transitions are red shifted. This red shift is expected to be a continuous function of the applied pressure, as far as phase transitions can be excluded. The pressure induced red shift of the phosphorescence band P of single-crystal NH_4–POP as observed at $T = 10$ K (cf. Figure 8) can be assigned to such a decrease of the intracomplex Pt–Pt distance *R*.

Another result of the application of high pressure is the occurrence of the additional phosphorescence band D, which has been observed for single-crystal NH_4–POP; cf. Figures 5 and 8. It can be traced back to the formation of oligomeric units (probably dimers) of $[Pt_2(POP)_4]^{4-}$ complex ions within the columns. If the crystal structure of the ammonium compound is similar to that of the potassium compound, as mentioned above, the formation of such oligomeric units should be within easy reach, since neighboring complex ions of a column have face-to-face positions and no other atoms are arranged between them. At sufficient approach of two $[Pt_2(POP)_4]^{4-}$ complex ions the $5d_{z^2}$ and the $6p_z$ orbitals of adjacent platinum(II) ions, respectively, will overlap and both the two degenerate LUMO's and the two degenerate HOMO's of the pair of complex ions will split energetically into four orbitals of the dimer $\{[Pt_2(POP)_4]^{4-}\}_2$, as shown in Figure 10. $\sigma[\sigma(p)]$ and $\sigma^*[\sigma^*(d)]$ are the LUMO (symmetry a_{1g}) and the HOMO (symmetry a_{2u}) of the dimer, respectively. Qualitatively similar results can be found straightforwardly for larger oligomeric units. By configuration interaction with states of corresponding symmetry the energy gap between the LUMO and the HOMO is reduced. With increasing pressure this gap decreases and the low-energy optical transitions will be red shifted by the same mechanism that yields the pressure-induced red shift of the band P. That agrees with the experimental result that the energy of the pressure-induced phosphorescence band D becomes lower with increasing pressure; cf. Figures 5 and 8.

That the phosphorescence spectrum of single-crystal Ba–POP exhibits another pressure dependence than that of NH_4–POP can be traced back to the different crystal structures. In the Ba–POP crystal the Pt–Pt axes of neighboring complex ions of a column are staggered, as shown in Figure 2. By high pressure the intercomplex distance within a column will be decreased. Because of the staggered arrangement of neighboring complexes, however, the intercomplex overlap between the $5d_{z^2}$ and $6p_z$ orbitals, respectively, is expected to be distinctly smaller than in a crystal with a linear arrangement of the Pt–Pt axes. Thus, the electronic energies of the oligomeric units differ only slightly from those of the monomers. As a consequence, the oligomeric band D cannot be resolved in the phosphorescence spectrum of single-crystal Ba–POP. Band D becomes noticeable only by an increase of both the half-width and the red shift of band P if the applied pressure is increased.

The decrease of the total phosphorescence intensity with increasing pressure is probably due to an enhancement of the coupling between the emitting centers and their surroundings, entailing an increase of nonradiative deactivation. The observed pressure dependence of the relative intensities of the band D and P (cf. Figures 5 and 8) indicates that the ratio of the numbers of emitting oligomers and monomers is a function of pressure (and temperature). The mechanism that controls this ratio is unknown as yet. Possibly the formation of emitting oligomeric units at high pressure can be reached only subsequently to the electronic excitation by a stabilization via a self-trap process.

Acknowledgment. This research has been supported by the Deutsche Forschungsgemeinschaft and the Fonds der Chemischen Industrie.